Agglomeration in PRATSOLIS Project

ANIMP
Multiphase Flow Engineering Section

POLITECNICO OF TURIN
Department of Material Science and Chemical Engineering

AIDIC
Italian Association of Chemical Engineering

Proceedings

Eighth International Conference

Multiphase Flow in Industrial Plants

Palazzo delle Mostre e dei Congressi
Alba, Cuneo, Italy
September 18-19-20, 2002

AGGLOMERATION IN PRATSOLIS PROJECT

M. Signorino, G. Baldi, A.A. Barresi, M. Cournil, J.J. Derksen, F. Gruy, E.D. Hollander, M. Kraume, D. Marchisio, A. Paschedag, M. Vanni, H.E.A. Van den Akker, A.M. Varone

341-371

ANIMP
Italian Association of Industrial Plant Engineering
Via Spalato 11/2 – 20124 Milan – Italy
Ph. +39 (2) 6070242
Fax +39 (2) 6070245
e-mail: anna@animp.it

Casa Editrice
ANIMP Servizi Srl
Via Spalato 11/2 – 20124 Milan – Italy

Pubblicazione realizzata da:
ELIO TICINESE PICKING PACK SERVICE POINT Srl
Via Venosa, 4/6 – 20137 Milan – Italy

ISBN
88-88198-03-02

SCIENTIFIC COMMITTEE

Giancarlo Baldi
Politecnico di Torino
Ugo Biliardo
Università "La Sapienza", Roma
Gian Piero Celata
Enea Casaccia, Roma
Giorgio Donsì
Università di Salerno
Dario Ercolani
Snamprogetti S.p.A., Centro di Fano
Sergio Fabbri
Università di Bologna
Giovanna Ferrari
Università di Salerno
Brunello Formisani
Università della Calabria
Francesco Ferrini
Techfem S.r.l., Fano
Giancarlo Giacchetta
Università di Ancona
Giovanni Guglielmini
Università di Genova
Carlo Lombardi
Politecnico di Milano
Barbara Mazzarotta
Università "La Sapienza", Roma
Agostino Mazzoni
ENI S.p.A. – Div. AGIP, Milano
Arrigo Pareschi
Università di Bologna
Cesare Saccani
Università di Bologna
Alessandro Terenzi
Snamprogetti S.p.A., Centro di Fano
Marco Vanni
Politecnico di Torino

ORGANIZING COMMITTEE

Giancarlo Baldi
Politecnico di Torino
Augusto Bianchini
Università di Bologna
Marco Bravi
Università di Roma
Marco Fossa
Università di Genova

Organizing Secretariat of the Conference
Anna Valenti, ANIMP, Milano

AGGLOMERATION IN PRATSOLIS PROJECT

M. Signorino, G. Baldi, A. A. Barresi, M. Cournil, J.J. Derksen, F. Gruy, E.D. Hollander, M. Kraume, D.Marchisio, A. Paschedag, M. Vanni, H.E.A. Van den Akker, A.M. Varone

PRATSOLIS Project:

Ecole des mines Saint Etiene (France)
Technische Universität Berlin (Germany)
Technische Universiteit Delft (The Netherlands)
Politecnico di Torino (Italy)

Abstract

The aim of this paper is to give an overview of the state of art in the agglomeration studies, and an introduction to the work carried out in this field, both from the numerical and the experimental point of view, by the European Network PRATSOLIS (PRecipitation and Agglomeration in Turbulent SOlid/LIquid Systems).

1. *Introduction*

In powder technology and industrial crystallization, agglomeration is known as an essential step because of its influence on the particle size and morphology. According to the desired quality of products or to possible process requirements, agglomeration should be prevented or promoted. For instance, agglomeration can be used to concentrate solid particles initially dispersed in a liquid medium, in order to make their withdrawal easier. Agglomeration, however, often appears as a step which should be avoided, especially when a suspension of a large population of very fine particles is to be produced. Meanwhile the understanding and mastering of agglomeration is an important challenge for technology and engineering. In this respect, several points deserve to be emphasized:

- Particle structure which induces particular geometrical, fluiddynamic, mechanical and optical properties.
- At all scales agglomeration involves a big variety of phenomena like solid particles interactions, morphology and mechanics of the agglomerates, fluiddynamic and chemical interactions between the flow and the agglomerates.
- The whole process of agglomeration is characterized by aggregation where the particles form cluster with a relatively loose structure, followed, in a supersaturated system, by crystal

particles of size *j*. According to the type of flow and the particle size, *Brownian* kernels or *turbulent* kernels should be considered. To express them, the relevant parameters are β_1, the ratio of the particle size to the *Kolmogoroff microscale* and β_2, the ratio of the particle size to the *Levich critical diameter* d_c [33].

For β_1 >1, models of highly turbulent suspensions should be applied [1].

For β_1 < 1 and β_2 >1, the classical turbulent models (which in fact assume a local shear flow in the Kolmogoroff's eddies) can be used.

For β_1 < 1 and β_2 < 1, the Brownian contribution is no more negligible. In this case, Adachi *et al.* [2] propose to express K_{ij} as the sum of two contributions:

$$K_{ij} = (K_{ij})_{Br} + (K_{ij})_{turb}$$

in which $(K_{ij})_{Br}$ is the Brownian kernel and $(K_{ij})_{turb}$ the turbulent kernel.

The problem is to describe the conditions of collision of two interacting particles brought into close proximity by a viscous fluid. At this scale, physicochemical interactions (van der Waals, double-layer,...) have an influence on the particle trajectories. Another, purely fluiddynamic, effect should be considered too. In fact, particles on intersecting trajectories will collide only if the liquid between them can be drained off to allow the contact. This results in a repulsive force (lubrication force) which can reduce or prevent agglomeration.

2.1.1 *Brownian motion*

Following the pioneering works of Smoluchowski [52], several authors [16;54] expressed the agglomeration flow J_{ij} (R) of particles of radius a_j which collide with the sphere of radius R surrounding a reference particle, of radius a_i:

$$J_{ij} = -4\pi R^2 G(R)\left[\left(D_i + D_j\right)\frac{\partial N_j}{\partial R} + \frac{N_j}{G\pi\mu}\frac{a_i + a_j}{a_i a_j}\frac{\partial V_T}{\partial R}\right] \qquad (1)$$

$G(R)$ (global collision efficiency) is a function of R, a_i and a_j; D_i is the Brownian diffusion coefficient of a sphere of radius a_i:

$$D_i = \frac{k_B T}{6\pi\mu a_i} \qquad (2)$$

in which a_i and a_j are the respective radii of particles *i* and *j* (supposed spherical) and α_{ij} the collision efficiency (see below).
An important parameter both in the agglomeration and the *breakage kernel* calculations is the *velocity gradient* $\dot{\gamma}$ which itself depends on the energy dissipation rate per unit mass ε_m. This is a local value but to get a rough approximations many expressions are found in the literature for the mean value of ε_m, for instance:

$$\overline{\varepsilon} = \frac{N_p \omega^3 D_s^5}{V} \qquad (5)$$

in which N_p is the power number, D_s the stirrer diameter, ω the rotation rate of the stirrer and V the volume of the suspension. This type of expression should be used with precautions because, ε_m is not uniform in a stirred vessel. This will be an essential subject of interest for the PRATSOLIS joint programme to get more realistic expressions for ε_m based on CFD computations, taking into account the local variations and the presence of solid particles in the flow.

2.2 Physico-chemical interactions between solid particles
The trajectories of the particles just before their encounter, the collision efficiency and the agglomerate cohesion, depend on the different interactions between solid particles. Two of them shall be discussed here:

- *London-Van der Waals attractive interactions*

These forces have their origin in interactions between instantaneous induced dipoles. For two spheres of radii a_i and a_j separated by distance h, an attractive interaction potential V_A can be calculated [21]. For instance, in the case of two identical particles of radius R, the interaction force F_w is given by :

$$F_w = \frac{AR}{12h^2} \qquad (6)$$

in which A is the *Hamaker constant* of the particle in the medium.

- Double layer repulsive interactions

A solid particle located in an electrolyte generally shows a surface charge and is surrounded by a layer of dissolved ions [59]. The zeta potential is the only characteristic parameter of this double layer which is experimentally

beginning of the agglomeration process, clusters are small and contain a few tenths of particles, even less; in this case, the fractal assumption is no more valid as well as the "macroscopic" models of large agglomerates.

2.4 *Agglomerate fragmentation*

The occurrence of break-up depends on the balance between the disagglomeration effects due to the action of the fluid and the overall cohesion of the agglomerate due to the interactions between primary particles. The fluiddynamic effects are of different nature if it is that the agglomerate is larger or smaller than the Kolmogoroff microscale. In the latter case, a shear stress originating from the local velocity gradient acts on the agglomerate. The different authors do not agree on the way to express the competition between the desagglomeration and the cohesion effects. According to the models, the relevant parameter is either the ratio $\frac{E_c}{E_t}$ or the ratio $\frac{\sigma}{\tau}$; E_c and E_t are respectively the agglomerate cohesion energy and the turbulent energy acting on this agglomerate; σ is the mean mechanical strength of the agglomerate and τ_s is the mean shear stress [53;4;32;36]. The breakage rate is proportional respectively to $\dot{\gamma}\, e^{\frac{E_c}{E_t}}$ and to $\dot{\gamma}\, e^{\frac{\sigma}{\tau}}$. Another discussion is related with size of the fragments produced by breakage. Two cases are currently envisaged:

- erosion of single or small groups of particles from the agglomerate surface;
- production of fragments with sizes of about one fourth of the agglomerate diameter.

In all cases, the breakage rate depends on the fluiddynamic conditions of the flow, via ε_m and μ and on the characteristics of the agglomerates: outer radius, fractal dimension, primary particle radius and cohesion force between two primary particles. This last parameter is calculated differently according to the nature of the bond between the particle and the rest of the agglomerate:

- in the case of purely physical interaction, it is equal to the van der Waals interaction;
- in the case of supersaturated solutions, crystalline bridges grow around the contact points, reinforce the aggregate cohesion and decrease the break-up probability [42];

density as the fractal agglomerate with the same primary particles number. Then, we may characterize a given agglomerates set by the previously defined and weak (in the mathematical meaning of the word) fractal dimension D_{wf}. This new definition can be only applied to agglomerates with high (quasi spherical) symmetry. The so-defined agglomerates contain accurately located primary particles. Hence, this description is more realistic than an enlargement of a fractal one to small agglomerates. During an agglomeration process, small and large agglomerates are present. If $i < i_{lim}$, agglomerates are assumed to belong to a given agglomerates set characterised by a weak fractal dimension D_{wf}; if $i > i_{lim}$, agglomerates are considered as fractal with the same fractal dimension. So, Gruy [19] defines several hierarchical families (sets) of agglomerates, each one characterised by its weak fractal dimension D_{wf}.

Another way to build agglomerate sets [20] consists of achieving computer simulation of agglomeration process: primary particles are randomly located on nodes of a cubic network and are allowed to move according to the shear flow; so, an agglomerates set is built. As the aim of these simulations is not the precise study of the whole agglomeration process or the particle size distribution determination at each time step, reasonable computer time is needed. As previously, a weak fractal dimension will be assigned to this agglomerates set.

3.2 *Physical properties of small agglomerates*

Each agglomerate is also characterised by its gyration radius, fluiddynamic radius, porosity, permeability, all physical parameters needed for modelling phenomena as sedimentation and agglomeration. Up to now, fluiddynamic behaviour of small (rigid or not rigid) agglomerates are not well understood. Recently Gruy [20] undertook to measure the sedimentation velocity of small agglomerates. They consist of a rigid set of glass beads (1mm in diameter). Various structures have been built: linear, planar or three-dimensional. The primary particles number per agglomerate is in the range (2-100). Settling was performed in glycerol in order to keep Reynolds number inferior to 0.1. So, we show that the fluiddynamic radius is equal to equivalent radius calculated from average projected area whatever is the orientation of the falling agglomerates.

Another important physical parameter for agglomerates is related to their experimental characterisation during agglomeration process. Characterisation of agglomerates population during agglomeration process is a difficult task. Unfortunately, no separation methods exist in order to classify a given population of loose agglomerates produced in a

The easiest way to determine the optical properties of an agglomerate is to calculate its effective refractive index m_a [14]. The equation derived by Maxwell-Garnett has proven to be suitable:

$$\frac{(m_a^2-1)}{(m_a^2+2)} = \bar{\phi}\,\frac{(m^2-1)}{(m^2+2)} \qquad (11)$$

m and m_a are the relative refractive indices respectively for primary particles and agglomerates.

Given the diameter and the effective refractive index of an agglomerate, the Mie theory allows to calculate the scattering cross section C_{sca} for a given wavelength.

- interferences method

Generally, the object (primary particle, agglomerate ...) can be divided into smaller identical parts (elements). Each element is polarisable. In the presence of a variable electric field, the element becomes an oscillating dipole, which itself creates an electromagnetic field. When an object is illuminated by an electromagnetic wave, each element receives the incident electric field and the one coming from the other elements. Thus, the object emits an electromagnetic wave (scattered wave), which includes the contribution of each oscillating dipole.

Most often, the incident wave is randomly polarised and the object (scatterer) can randomly orientate. Thus, the optical properties are obtained after calculating an average over all the wave polarisation states and object orientations.

Table 1 presents several models, each one characterised by the polarisable element, the object, the calculation type. If the object is an agglomerate, the element may be either the whole primary particle or a part of the primary particle. The Khlebtsov procedure, similar to Percival-Berry [6] one, has been applied to agglomerates of many particles (fractal agglomerates).

For instance, agglomeration of silica suspension has been studied [19]. The m value (silica in water) is close to 1 ($m-1 \ll 1$). Depending on the primary particle size, two cases are possible :

agglomeration was carried out in a stirred tank under physicochemical conditions corresponding to attractive inter-particle forces. The effect of different primary particle sizes and stirring rates on agglomeration dynamics has been studied. Agglomeration has been studied by using:

- Kusters's approach for collision efficiency calculation [32]
- Brakalov's approach for agglomeration-fragmentation dynamics at high time [7].

It has been showed that:

- agglomerates are small in a stirred tank (primary particle number per agglomerate smaller than 100)
- small agglomerates are slightly porous. Several agglomerates sets and their equivalent or weak fractal dimension D_{wf} have been defined, which is found in the range (2.4-2.5). This is also verified for the beginning of Brownian agglomeration.
- agglomeration process is characterised by D_{wf} and agglomerate limit size L.
- D_{wf} (respectively L) is a weakly increasing (respectively decreasing) function of the stirring rate or of the shear rate.

4. *Population Balance*

The simulation of a dispersed system often requires the solution of the population balance, that is, a budget equation (or set of equations) for the particle distribution function, which accounts for all the processes that generate, enlarge or remove particles from the population [25]. In the population balance particulate properties are represented by a set of internal and external coordinates. External coordinates refer to the spatial location of the particles and internal coordinates to their intrinsic properties, such as size, surface area, void fraction, shape factor, etc. Mathematically the population balance equation is expressed by an integro-differential equation for continuous populations or by its discrete counterpart, if the population is discrete (as it may occur for aggregation-breakage processes in the absence of particle growth). For populations of small particles, as those normally present in turbulent precipitation processes, it can be assumed that the particles have exactly the same velocity as the fluid. In this case the population balance for an inhomogeneous turbulent system with particle size as the only internal coordinate becomes:

The choice depends on a number of factors: number of internal coordinates, complexity of the mechanisms of aggregation, breakage and growth, computational load, role of non-homogeneity in the system, ease of implementation. In the following the three methods will be shortly reviewed, in order to illustrate the proper field of application of each one.

4.1 *The moment method*

In the standard moment method (SMM) the internal coordinate is integrated out and the population is described in terms of its moments:

$$m_j = \int_0^\infty n(L)\, L^j\, dL \qquad (19)$$

In this way the integral properties of the population are an immediate outcome of the method: the zeroth moment giving the total particle number, the second one being related to the total surface area, the third one to the total particle volume or mass. This type of information may be sufficient for many purposes and, if this is the case, the moment method can be very effective.

In order to obtain an equation for the *j*-th moment, Eq. (1) is multiplied for L^j and integrated over *L*. The resulting equations have the same structure as the scalar transport equations of Computational Fluid Dynamics and thus they can be coupled easily with CFD codes, as done, for instance, by Marchisio *et al.* [39] in their study on barium sulphate precipitation. The main advantage of the method is that the number of equations required (and therefore of calculated moments) is very small, usually from 4 to 6. The disadvantage is that these equations form a closed set only if the rate of growth and the aggregation and breakage kernels are size-independent. The problem has been recently overcome by the Quadrature Method of Moments (QMOM), proposed originally by McGraw [37]. Here particular quadrature formulas are used that make it possible to express the growth, birth and death rate appearing in the budget equation of each moment in terms of lower order moments only. The QMOM has been recently applied to processes of aggregation and breakage and has shown to be able to give very accurate predictions of the main integral properties of a population, even for conditions at which more computationally intense sectional methods fail [39].

4.2 *Method of classes*

Sectional methods divide the size range in a number of sections and apply a balance equation to each of the formed intervals. As evidenced by Kumar and Ramkrishna [46], sectional methods can be derived through a

4.3 *Direct Simulation Monte Carlo method*

The methods cited so far consider size as the only internal coordinate. Unfortunately many processes lead to the consideration of two or more internal variables. Occasionally multi-dimensional extensions of the previous methods have been adopted: Xiong and Pratsinis [67] and Jackson [26] for the method of the classes and Wright *et al.* [65] for the QMOM. Although these papers refer to coagulation processes with simple kinetics and two internal coordinates only, the implementation resulted in a very complex algorithm. Therefore it does not seem practical to extend these approaches to a higher number of internal coordinates.

An alternative is Monte Carlo simulation. In this case an artificial realisation of the studied process is created, by generating a sequence of random events on a computer, which obeys the same statistical laws as the physical system. This technique is often indicated as the DSMC [pope] (Direct Simulation Monte Carlo) method. The DSMC method is based exclusively on the transformation of event rates (*i.e.* aggregation or breakage rate) in event probabilities, without regarding the actual particle movements or trajectories. Figures 1 and 2 show the outcomes of the classes method and of the DSMC approach, respectively, for the same conditions, evidencing the statistical nature of the latter.

Monte Carlo simulations are computationally expensive, since a large number of simulated particles (10^4 to 10^6 in a homogeneous system) should be used, in order to obtain accurate results. Due to this fact, at present the method cannot be coupled with classical CFD codes to analyse processes in non-homogeneous systems, whereas a coupling with Lattice-Boltzmann solvers seams to be reasonable.

In comparison with the previous approaches, the Monte Carlo method obviates the need for solving integro-differential equations, which become exceedingly difficult for multivariate number density functions. The implementation of multidimensional systems does not give relevant additional problems to the DSMC approach. Furthermore, since the Monte Carlo method is based on the generation of a sequence of particular events, it is easy to consider complex aggregation or fragmentation mechanisms that, conversely, may be difficult to implement in the analytical form required by the population balance equations.

Another advantage of the DSMC method is that information about the history of the particles is available. This fact makes Monte Carlo simulation a valuable tool to predict the internal structure of the formed aggregates, that is determined by the sequence and the type of the collisions.

(c)). For high values (α=3) aggregation plays an important rule resulting in a significantly different structure (Figure 4, (d)).
Results of experiments at high concentrations are reported in Figure 5. As it is possible to see, for all values of α, the CSDs maintain the same shape, although generally the primary peak decreases and the secondary one (or ones) increases. This is a proof of the high tendency of the precipitate to aggregate also for longer time (30 min). It should be highlighted that in this case also at the reactor outlet CSDs had more than one peak, meaning that aggregation started to occur inside the reactor despite the short residence time.
The simulation results presented here were gained with commercial codes (Fluent, Star-CD), where the fluid dynamic field is solved via standard κ–ε turbulence model already implemented in the code, while the micromixing and the population balance model were introduced via user-defined functions.
After solving the flow field to get mean velocities and turbulence quantities in stationary conditions two methodologies were followed.
The first approach is constituted by a set of nine transport equations, in which the convection and the turbulent diffusion were modelled by the CFD code, and a source term must be specified for each scalar. Mixing properties were determined by solving the transport equations for the probability of modes (concentration of the reactant species at the inlet) A and B and for the weighted mixture fraction and high concentration ratio values. The reaction and particles formation were given by solving the transport equation for the reaction progress variable and for the CSD moments the Standard Moments Method was used.
For the second approach to solve the CSD the class method was used with a total number of 40 classes, while the discretization of agglomeration term was done with the method presented in [10] which allows conservation of particles and mass number.
In Figure 6 model predictions at the reactor outlet are compared with experimental data (high concentration, c_{A0}=34mol/m^3, α=3.0). The mean crystal size is compared with the model with and without aggregation. In this case only a constant kernel is considered for agglomeration. Comparison shows that for these operating conditions if aggregation is neglected the mean crystal size is significantly underestimated, for α larger than 0.1. The mean crystal size of agglomerates is still higher than model predictions. This could be caused by the fact that turbulent aggregation is not considered. In fact, it has been shown that also for particles smaller than the Kolmogorov scale turbulent aggregation might be important.
Figure 7 shows the normalized integral particle size distribution for the experiments and for the different computations (c_{A0}=0.0049kg/kg,

apparent. The vortical structures of various sizes that can be observed in the snapshot are lost in the time-averaged flow. The availability of local, and time-dependent flow information in an LES, as demonstrated in Figure 10, is exactly the reason why it has been used in our study on the interaction between agglomeration and turbulence. The non-linear relation between the agglomeration and the shear rate (Figure 8) requires local shear rate information, and not average information, since $K(\bar{\dot{\gamma}}) \neq \overline{K(\dot{\gamma})}$ (where an overbar indicates spatial and/or temporal averaging).

In order to model agglomeration in stirred tanks, the LES code was supplemented with a Monte-Carlo algorithm that solved the transport equation for the number density n [23]. In the transport equation, agglomeration acts as a sink. The local, time-dependent shear rate, necessary to determine the local value of K in the particle number transport equation was estimated from the LES through the deformation rate:

$$\dot{\gamma}^2 \approx 2S_{ij}S_{ij} \equiv \frac{1}{2}\left(\frac{\partial u_i}{\partial x_j} + \frac{\partial u_j}{\partial x_i}\right)^2 \qquad (20)$$

The size of the particles (typically 10 μm) justifies a one-way coupling assumption (i.e. the crystals feel the turbulent fluid flow, the fluid does not feel the presence of the crystals), since the particles are smaller than the Kolmogorov length scale. The presence of the particles might slightly increase the apparent viscosity of the tank's content (through the Einstein-relation for suspension viscosities, see also Hollander [23]).

A sample simulation result is presented in Figure 10. It shows for the specific $CaOx{\cdot}H_2O$ system (with β as depicted in Figure 8) the (obviously inhomogeneous) distribution of the agglomeration rate kernel throughout the tank. The time-averaged part of Figure 10 indicates that hardly any agglomeration occurs in the volume swept by the impeller. Apparently shear rates close to the impeller are too high to cause agglomeration. The single-realization shows how the turbulent flow structures translate into a spatial K-distribution.

With the numerical tool described above, a large number of cases (25 in total) has been simulated [23]. Three scale-up rules (constant specific power input, constant tip-speed, and constant Reynolds number) have been applied to tanks ranging in size from 10^{-3} m^3 to 10 m^3 equipped with two different impellers (*viz.* a Rushton turbine, and a 45° pitch-blade turbine with four blades). One number has characterized the result of every individual simulation: the apparent agglomeration rate kernel, which is a measure for the tank-averaged agglomeration behavior. The apparent agglomeration

For the solution of the population balance mainly three different techniques can be used: The momentum method; The method of classes; The Monte Carlo method.
The own results presented regard precipitation in a tubular reactor and in a stirred vessel. The tube has been modelled by combining population balance solver with commercial CFD codes, using the momentum method
For the stirred tank Lattice-Boltzmann simulations with LES for the turbulent flow have been combined with Monte Carlo simulations
Apart from focusing a validating and/or determining kinetics, work needs to be done to refine the simulation.

References

[1] Abrahamson, J.(1975), Collision rates of small particles in a vigorously turbulent fluid, Chem. Eng. Sci., 30, 1371
[2] Adachi, Y., Cohen Stuart, M. A., and Fokkink, R. (1994), Kinetics of Turbulent Coagulation Studied by Means of End-over-End Rotation J. Coll. Interface Sci., 165, 310-317.
[3] Aoun, M., E. Plasari, R. David, and J. Villermaux, "Are barium sulphate kinetics sufficently known for testing precipitation reactor models?", Chem. Eng. Sci., 51, 2449 (1996).
[4] Ayazi Shamlou, P., Stavrinides, S., Titchener-Hooker, N., Hoare, M. (1994), Growth-independent breakage frequency of protein precipitates in turbulently agitated bioreactors. Chem. Eng. Sci., 49, 2647.
[5] Batterham, R.J., Hall, J.S., and Barton, G., *Proc. 3rd International Symposium on Agglomeration*, Nurnberg, A136 (1981).
[6] Berry, M.V., Percival, I. C., Optica Acta 33, 577 (1986)
[7] Brakalov, L.B., Chem. Eng. Sci., 42, 2373 (1987).
[8] Crawley, G. M., Cournil, M., and Di Benedetto, D., Powder Technology, 91, 197 (1997).
[9] De Boer, G. B. J., Hoedemakers, G. F. M., Thoenes, D. (1989). Coagulation in turbulent flow. Chem. Engng. Res. Des., 67, 301-315.
[10] Cresswell, P.J. , F.E. Harig, R.R.M. Johnston, G.M. Leigh and J.A. Thurlby, Modelling Alumina Trihydrate Precipitation - Prediction of Laboratory Kinetic and Size Data, 6th AusIMM Extractive Metallurgy Conference, Brisbane, 3-6 July 1994.
[11] Derjaguin, B. V., Landau, L. (1941),. Acta Physiochim. URSS 14, 633.
[12] Derksen, J.J., and Van den Akker, H.E.A., Large eddy simulations on the flow driven by a Rushton turbine. AIChE J. 45 (1999) 209-221.
[13] Di Stasio S., Massoli P., Partec 98, 7th European Symposium Particle Characterization I, 169 (1998).
[14] Draine, B. T., Flatau, P. J., J. Opt. Soc. Am. 11, 1491 (1994)

[40] Marchal, P., David, R., Klein, J.P., and Villermaux, J., *Chem. Eng. Sci.* **43**, 59 (1988).
[41] Meakin, P., "The growth of fractal aggregates", in Time-Dependent Effects in Disordered Materials (R. Pinn and T. Riste, eds), 45. Plenum Press, New York (1987).
[42] Mulholland, G. W., Bohren, C. F., Fuller, K. A., Langmuir 10, 2533 (1994)
[43] Mumtaz, H.S., Hounslow, M.J., Seaton, N.A., Paterson, W.R. (1997), Orthokinetic aggregation during precipitation: a computional model for calcium oxalate monohydrate. Trans. Instn Chem. Engng, 75, Part A, 152-159.
[44] Oles, V. (1992), Shear-induced aggregation and breakup of polystyrene latex particles.
[45] Paschedag, A, Tornatora, M., Auser, Ilja, ..., Modelling of Agglomeration for $BaSO_4$ Precipitation. to be presented at the 15th Symp. On Industrial Crystallisation, Sorrento, 15-18/9/2002.
[46] Ramkrishna, D., Rev. Chem. Eng. 3, 49 (1985).
[47] Ruckenstein, E., Churaev, N. (1991), A possible fluiddynamic origin of the forces of hydrophobic attraction. J. Colloid Interface Sci., 147(2), 535-538.
[48] Saffman, P. G., Turner, J. S., (1956), On the collision of drops in turbulent clouds, J. Fluid Mech., 1, 16-30.
[49] Saint-Raymond, H., Gruy, F., Cournil, M. (1998). Turbulent aggregation of alumina in Water and n-Heptane, J. Colloid Interface Sci., 202, 238-250.
[50] Shah, B.H., Ramkrishna, D. and Borwanker, J.D., AIChE J., 23, 897 (1977).
[51] Smagorinsky J., General circulation experiments with the primitive equations: part I, the basic experiment. Monthly Weather Rev. 91(1963) 99-164.
[52] Smoluchowski, M., Z. (1917), Mathematical theory of the kinetics of the coagulation of colloidal solutions. Z. Physik. Chem., 92, 129.
[53] Sonntag, R. C., and Russel, W. B., (1987), J. Coll. Interface Sci., 115, 378.
[54] Spielman, L. A. (1970). Viscous interactions in brownian coagulation. J. Coll. Inter. Sci., 33, 562.
[55] Tandon, P., and D.E. Rosner, J. Colloid Interface Sci., 213, 273 (1999).
[56] Tontrup, C., Gruy, F., Cournil, M., J. Colloid and Interf. Sci., 229, 511 (2000).
[57] Torres, F. E., Russel, W. B., Schowalter, W. R., J. Coll. Interface Sci., 142, 554 (1991).

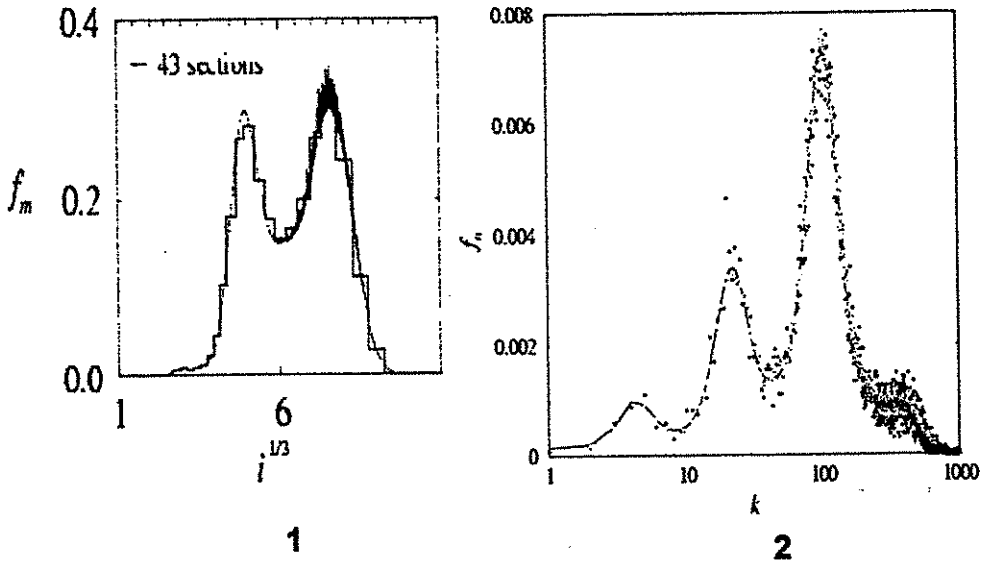

Figure 1: Asymptotic PSD for an aggregation-breakage process with fragment mass ratio 4:1. Thick line: prediction of the classes method by Kumar and Ramkrishna; thin line: rigorous solution.

Figure 2: Asymptotic PSD for the same situation as reported in Figure 1 predicted by a DSMC approach

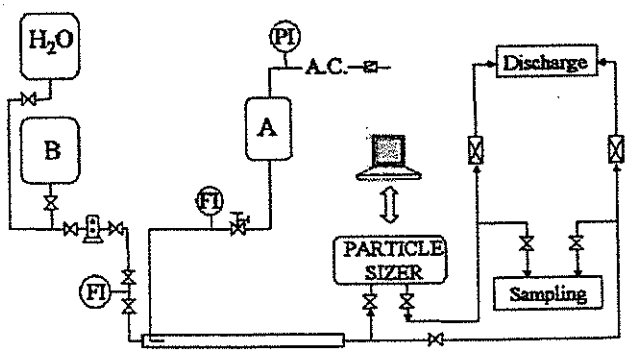

Figure 3: Experimental set-up (Politecnico di Torino)

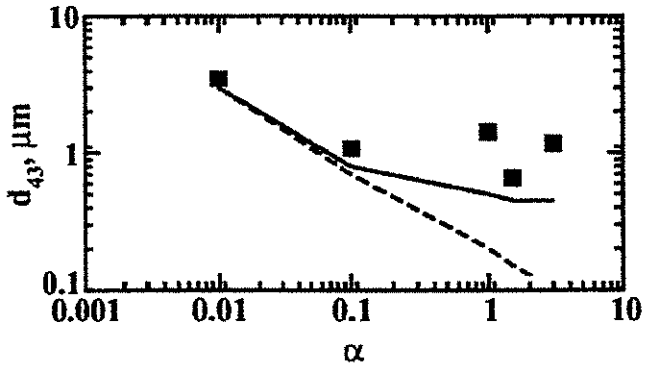

Figure 6: Mean crystal size versus α (solid line: model prediction; dashed line: model prediction neglecting aggregation).

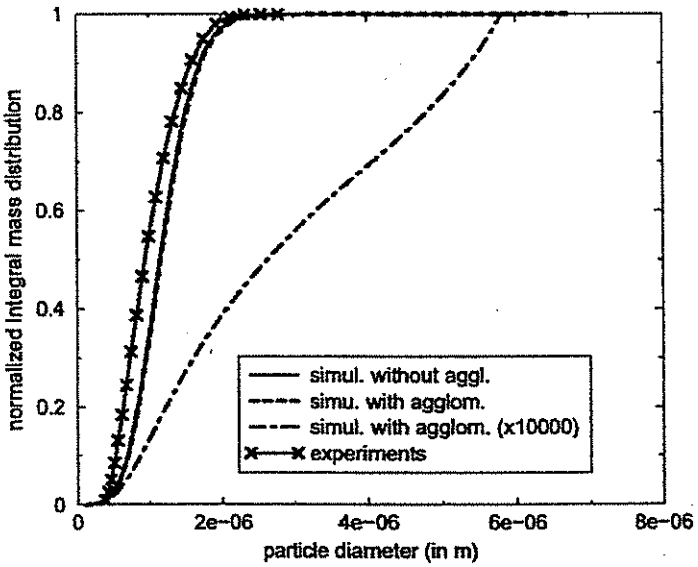

Figure 7: comparison of numerical results with and without agglomeration with experimental one.

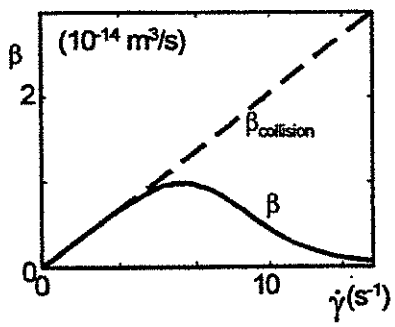

Figure 8: The agglomeration kernel β (as defined in Equation 1) in simple shear flow as a function of the shear rate, theoretical model due to Mumtaz *et al.* (1997) for $CaOx{\cdot}H_2O$ crystals. For reference, the collision kernel $\beta_{collision}$ is indicated.

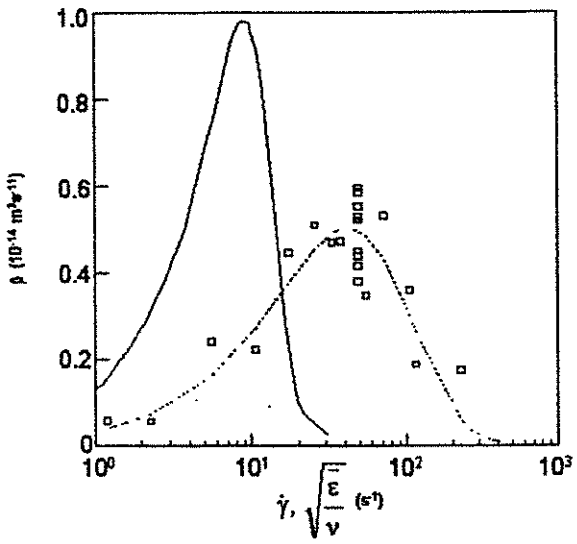

Figure 11: Solid line: same as Figure 9, with $\dot{\gamma}$ on a logarithmic scale. Symbols: tank-averaged agglomeration kernels (various tank sizes and impeller geometries) as a function of the tank-averaged shear rate $\sqrt{\frac{\bar{\varepsilon}}{\nu}}$. Dashed line: fit through the symbols with the same mathematical expression as used for the solid line.

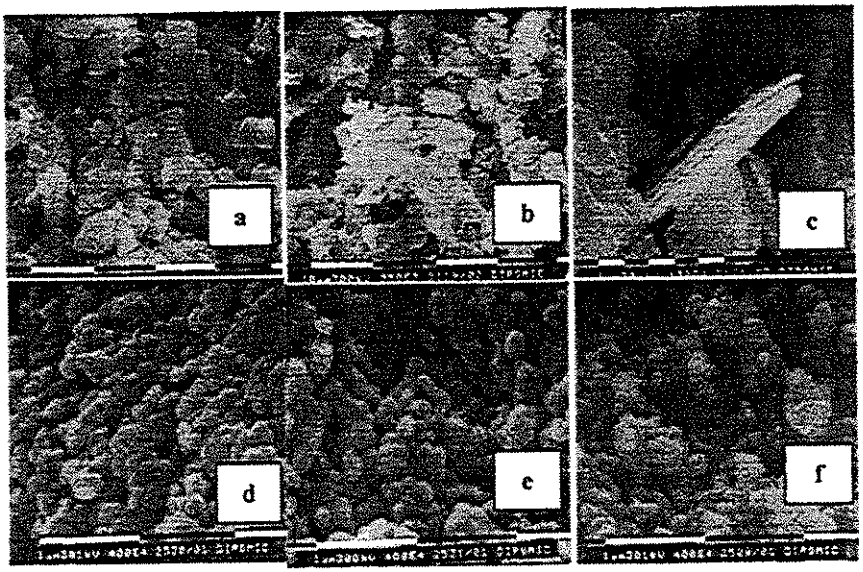

Figure 4: Crystal morphologies: a) tabular crystals ($BaCl_2$ in the jet c_{A0} =34 mol/ m^3 , α=0.1); b) dendritic crystals($BaCl_2$ in the jet c_{A0} =34 mol/ m^3 , α=1.0); c)particular of a dendritic crystal in (b) conditions; d) round-shaped crystals ($BaCl_2$ in the jet c_{A0} =34 mol/ m^3 , α=3.0); e) round-shaped crystals (Na_2SO_4 in the jet c_{A0} =34 mol/ m^3 , α=3.0); f) round-shaped crystals ($BaCl_2$ in the jet c_{A0} =341 mol/ m^3 , α=0.1).

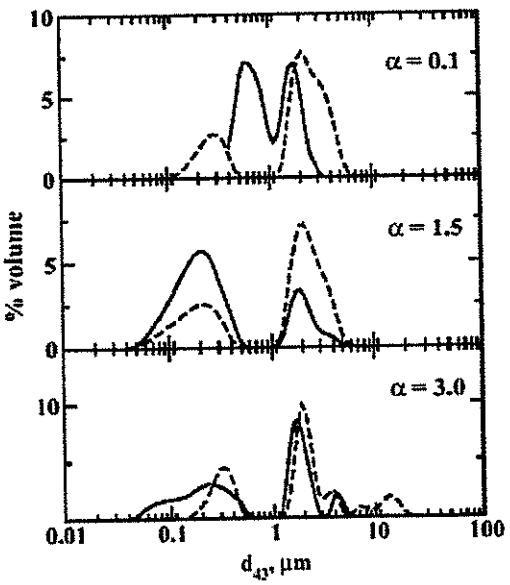

Figure 5: CSDs for several values of α at the reactor outlet (solid line) and after 30 minutes of gentle stirring (dashed lines).

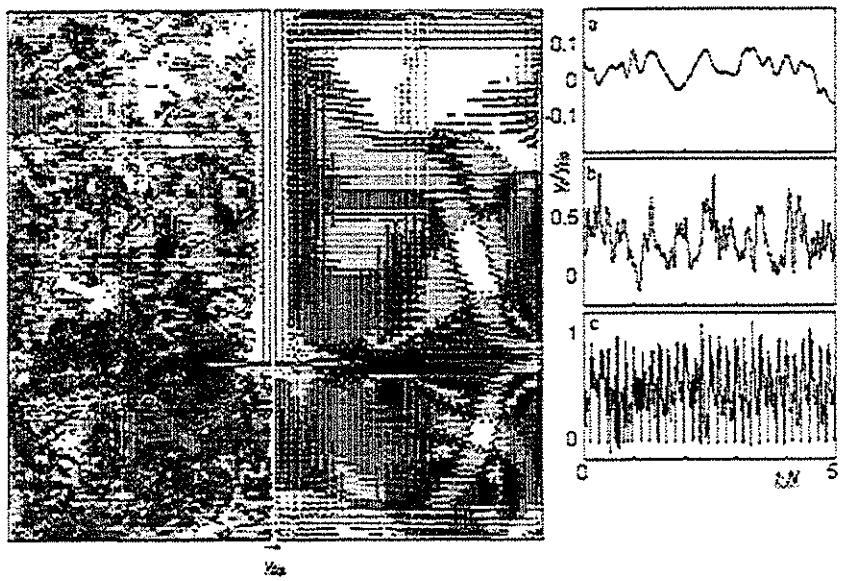

Figure 9: Left: a snapshot of the flow driven by the Rushton turbine in a vertical plane midway between two baffles. Center: the average flow field (averaging time: 24 impeller revolutions) in the same plane. Right: three velocity time series at different positions in the tank (as indicated in the center figure). The grid size was 180^3, the Reynolds number amounted to 29,000.

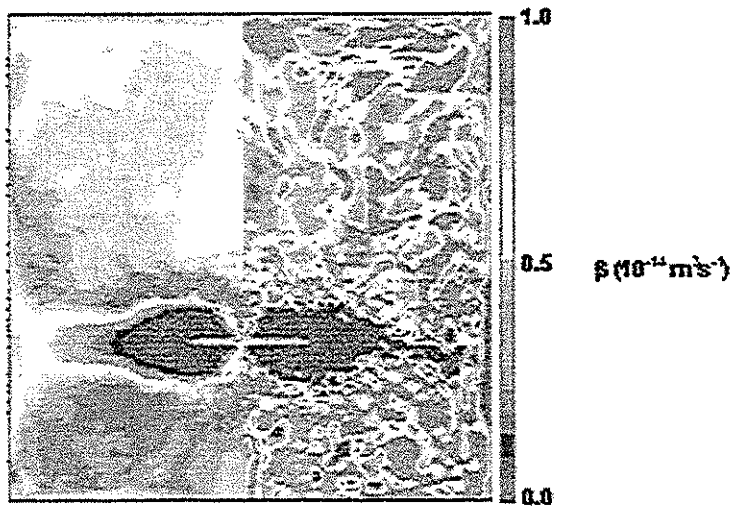

Figure 10: Typical distribution of the agglomeration kernel β throughout the vertical plane midway between two baffles in an agitated tank driven by a Rushton turbine. Left: time-averaged values; right: single realization.